

High-scale validity of a two Higgs doublet scenario: predicting collider signalsNabarun Chakrabarty^{†1} and Biswarup Mukhopadhyaya^{*2}*Regional Centre for Accelerator-based Particle Physics**Harish-Chandra Research Institute, HBNI,**Chhatnag Road, Jhansi, Allahabad - 211 019, India***Abstract**

It is possible to ameliorate the Higgs vacuum stability problem by switching over to two Higgs doublet models (2HDM), ensuring a stable electroweak vacuum up to the Planck scale, even though the top quark mass may be on the high side. However, the simultaneous requirements of perturbative unitarity, and also compatibility with collider and flavour data, constrain the parameter space severely. We investigate the collider signals answering to the regions allowed by such constraints. In particular, the near degeneracy of the neutral heavy scalar and the pseudoscalar is a feature that is probed. The LHC allows distinguishability of these two states, together with signal significance of at least 3σ , in its high-luminosity run. While e^+e^- colliders may have rather low event rates, muon colliders, cashing on the principle of radiative return, can probe 2HDM scenarios with (pseudo)scalar masses up to a TeV or so, though with the price of losing distinction between the CP-even and odd states.

¹nabarunc@hri.res.in²biswarup@hri.res.in

1 Introduction

The spin-0 particle of mass around 125 GeV discovered by the ATLAS [1] and CMS [2] collaborations at the Large Hadron Collider (LHC) apparently completes the particle spectrum of the Standard Model (SM). Moreover, the couplings of this particle to the other SM particles are progressively getting closer to the corresponding SM values. However, issues ranging from the presence of dark matter in the universe to the naturalness problem of the electroweak scale keep alive the hope of finding physics beyond the SM (BSM). While the search for such new physics remains on, a rather pertinent question is to ask whether the SM by itself can ensure vacuum stability at scales above that of electroweak symmetry breaking (EWSB). This is because the Higgs quartic coupling evolving via SM interactions alone tends to turn negative in between the Electroweak (EW) and Planck scales, thereby making the scalar potential unbounded from below. This is particularly true if the top quark mass is on the upper edge of its allowed band [3, 4]. While a *metastable* EW minimum remains a possibility, stabilising the EW vacuum calls for the introduction of additional bosonic fields preferably by extending the SM Higgs sector. A number of scenarios comprising new physics are suggested for retrieving vacuum stability, a representative list of which is [5–11]. One important demonstration in this context is that stability till the Planck scale is restored, irrespective of the top-mass uncertainty, just by switching over to two Higgs doublet models (2HDM). 2HDMs open up a world of enriched collider phenomenology, CP-violation from the scalar sector and also dark matter candidates in special cases.

However, a challenge faced while alleviating the vacuum instability problem using 2HDMs (or any extended Higgs sector for that matter) is that the quartic couplings so introduced tend to become non-perturbative while evolving under renormalisation group (RG). A balance between these two extremes is struck through judicious boundary conditions, which in turn leads to strong constraints on the masses and mixing angles. Elaborate accounts of this can be found in recent works. Two important points emerge from such studies. First, the spectrum of the non-standard scalars allows for only a small splitting. Secondly, the couplings of the 125 GeV Higgs with gauge bosons should have rather small deviation from the SM values. On the other hand, the gauge interactions of the non-standard scalars become suppressed.

In this work, we aim to investigate the observability of a 2HDM at the present [12–20] and upcoming colliders [21, 22] within the parameter region that allows for high-scale validity (including both vacuum stability and perturbativity). This could turn challenging since the search prospects could be severely inhibited by the constraints. For instance, to discern a 2HDM from the SM background through resonances, fully reconstructible final states need to be looked at. The corresponding event rates tend to be small, owing to the constraints on the interaction strengths that come from demanding the dual requirement of high scale vacuum stability and perturbative unitarity. Moreover, removal of the backgrounds requires event selection criteria which further lower the signal strength.

To be more specific, the CP-even heavier neutral Higgs could lead to a four-lepton cascade at the LHC via the ZZ state. Side by side, the CP-odd scalar leaves its signature in the completely reconstructible channel hZ where h denotes the SM-like Higgs. The two final states mentioned above are indicative of the opposite CP-properties of the decaying Higgses, which from our requirement, are destined to have closely spaced masses. We adopt a cut-based analysis to calculate the statistical significance in the respective signals. We perform this analysis for both Type-I and Type-II 2HDM. The allowed parameter space for the latter scenario is obtained via extensive investigation in reference [23]. For the former, though an analysis is found

in [24], for the sake of completeness, we present a set of results here that go beyond what has been reported. It is found that the constraints from flavour changing neutral current (FCNC) phenomena put a strong lower limit on the Type-II 2HDM charged scalar mass (and, via the correlation demanded by high-scale validity, on the heavy neutral scalar and pseudoscalar masses as well). Thus while obtaining LHC signals, the region of the parameter space in the Type-II case is relatively more restricted. Keeping this in mind, we also present a brief discussion on the prospects at other types of colliders. In particular, we find that muon colliders can be useful in this respect.

This study comprises of the following parts. In section 2, we briefly review the 2HDM and survey its candidature as a UV-complete scenario. Section 3 highlights the intrinsic features of the parameter space that permits high-scale stability. The search prospects at the LHC, and, future leptonic colliders are elaborated in sections 4 and 5 respectively. We summarise our findings and conclude in section 6.

2 2HDM and high scale validity.

Type-I and II 2HDMs, as well as the constraints on them have already been discussed in literature [25]. We present a small resume here for completeness. We consider the most general renormalizable scalar potential for two doublets Φ_1 and Φ_2 , each having hypercharge (+1):

$$\begin{aligned} V(\Phi_1, \Phi_2) = & m_{11}^2 \Phi_1^\dagger \Phi_1 + m_{22}^2 \Phi_2^\dagger \Phi_2 - m_{12}^2 \left(\Phi_1^\dagger \Phi_2 + \Phi_2^\dagger \Phi_1 \right) + \frac{\lambda_1}{2} \left(\Phi_1^\dagger \Phi_1 \right)^2 + \frac{\lambda_2}{2} \left(\Phi_2^\dagger \Phi_2 \right)^2 \\ & + \lambda_3 \Phi_1^\dagger \Phi_1 \Phi_2^\dagger \Phi_2 + \lambda_4 \Phi_1^\dagger \Phi_2 \Phi_2^\dagger \Phi_1 + \frac{\lambda_5}{2} \left[\left(\Phi_1^\dagger \Phi_2 \right)^2 + \left(\Phi_2^\dagger \Phi_1 \right)^2 \right] \\ & + \lambda_6 \Phi_1^\dagger \Phi_1 \left(\Phi_1^\dagger \Phi_2 + \Phi_2^\dagger \Phi_1 \right) + \lambda_7 \Phi_2^\dagger \Phi_2 \left(\Phi_1^\dagger \Phi_2 + \Phi_2^\dagger \Phi_1 \right). \end{aligned} \quad (2.1)$$

We parametrise the doublets as

$$\Phi_i = \frac{1}{\sqrt{2}} \begin{pmatrix} \sqrt{2} w_i^+ \\ v_i + h_i + i z_i \end{pmatrix} \text{ for } i = 1, 2. \quad (2.2)$$

One defines $\tan\beta = \frac{v_2}{v_1}$. In such a case, the scalar spectrum consists of a pair of neutral CP even scalars (h, H), a CP odd neutral scalar (A) and a charged scalar (H^\pm). The mass matrices are brought into diagonal form by the action unitary matrices comprising of mixing angles α and β . This scenario in general allows for CP-violation in the scalar sector [26–28], through the phases in m_{12} and λ_5 . However, this would lead to a contamination of our proposed search channels due to interference effects coming from $H - A$ mixing. Thus we restrict ourselves to a CP conserving scenario only.

A particular fermion generation can couple to both Φ_1 and Φ_2 in a 2HDM without violating the gauge symmetry. However, this leads to flavour changing neutral currents (FCNC) mediated by the Higgses, which are tightly constrained by experimental data. A manner to annul the FCNCs is to adhere to specific schemes of Yukawa interactions [29, 30], that are consequences of discrete symmetries. An example is the \mathbb{Z}_2 symmetry under which $\Phi_1 \rightarrow -\Phi_1$ and $\Phi_2 \rightarrow \Phi_2$. This demands $m_{12}, \lambda_6, \lambda_7 = 0$. Assigning appropriate \mathbb{Z}_2 charges to the fermions gives rise to the celebrated Type-I and Type-II models [25]. While the primary motivation of the above is to suppress flavour changing neutral currents (FCNC) [31–33], it reduces the number of free parameters in the Yukawa sector.¹ This also simplifies the expressions for the one-loop beta functions. Note

¹It was reported in [34] that the FCNCs are stable under Renormalisation Group.

that one could introduce Z_2 violation in the scalar potential only. This would ultimately lead to FCNC, however which would be radiatively suppressed. In this study, we consider both the cases of an exactly \mathbb{Z}_2 symmetric 2HDM, and one that violates it in the scalar potential.

We choose $\{\tan\beta, m_h, m_H, m_A, m_{H^\pm}, m_{12}, c_{\beta-\alpha}, \lambda_6, \lambda_7\}$ as the set of independent input parameters. The rest of the quartic couplings are expressed in terms of which for convenience. With $v = 246$ GeV and writing $c_\alpha = \cos\alpha$, $s_\alpha = \sin\alpha$, the remaining couplings can be expressed as

$$\lambda_1 = \frac{1}{v^2 c_\beta^2} \left(c_\alpha^2 m_H^2 + v^2 s_\alpha^2 m_h^2 - m_{12}^2 \frac{s_\beta}{c_\beta} - \frac{3}{2} \lambda_6 v^2 s_\beta c_\beta - \frac{1}{2} \lambda_7 v^2 \frac{s_\beta^3}{c_\beta} \right), \quad (2.3a)$$

$$\lambda_2 = \frac{1}{v^2 s_\beta^2} \left(s_\alpha^2 m_H^2 + v^2 c_\alpha^2 m_h^2 - m_{12}^2 \frac{c_\beta}{s_\beta} - \frac{3}{2} \lambda_7 v^2 s_\beta c_\beta - \frac{1}{2} \lambda_6 v^2 \frac{c_\beta^3}{s_\beta} \right), \quad (2.3b)$$

$$\lambda_4 = \frac{1}{v^2} (m_A^2 - 2m_{H^\pm}^2) + \frac{m_{12}^2}{v^2 s_\beta c_\beta} - \frac{1}{2t_\beta} \lambda_6 - \frac{1}{2} t_\beta \lambda_7, \quad (2.3c)$$

$$\lambda_5 = \frac{m_{12}^2}{v^2 s_\beta c_\beta} - \frac{m_A^2}{v^2} - \frac{1}{2t_\beta} \lambda_6 - \frac{1}{2} t_\beta \lambda_7, \quad (2.3d)$$

$$\lambda_3 = \frac{1}{v^2 s_\beta c_\beta} ((m_H^2 - m_h^2) s_\alpha c_\alpha + m_A^2 s_\beta c_\beta - \lambda_6 v^2 c_\beta^2 - \lambda_7 v^2 s_\beta^2) - \lambda_4. \quad (2.3e)$$

The mass parameters m_{11} and m_{22} in the scalar potential are traded off using the EWSB conditions. A given set of input parameters serves as boundary conditions for λ_i for the analysis using RG equations. While carrying out the analysis, several constraints coming from both theory and experiments must be satisfied.

2.0.1 Perturbativity, unitarity and vacuum stability

For the 2HDM to remain a perturbative theory at a given energy scale, one requires $|\lambda_i| \leq 4\pi$ ($i = 1, \dots, 5$) and $|y_i| \leq \sqrt{4\pi}$ ($i = t, b, \tau$) at that scale. This translates into upper bounds on the model parameters at low as well as high energy scales.

The matrix containing $2 \rightarrow 2$ scattering amplitudes of longitudinal gauge bosons can be mapped to a corresponding matrix for the scattering of the goldstone bosons [35–38], by virtue of the EW equivalence theorem. The theory is deemed unitary if each eigenvalue of the aforementioned amplitude matrix does not exceed 8π . The expressions for the eigenvalues are given below.

$$a_\pm = \frac{3}{2}(\lambda_1 + \lambda_2) \pm \sqrt{\frac{9}{4}(\lambda_1 - \lambda_2)^2 + (2\lambda_3 + \lambda_4)^2}, \quad (2.4a)$$

$$b_\pm = \frac{1}{2}(\lambda_1 + \lambda_2) \pm \sqrt{\frac{1}{4}(\lambda_1 - \lambda_2)^2 + \lambda_4^2}, \quad (2.4b)$$

$$c_\pm = d_\pm = \frac{1}{2}(\lambda_1 + \lambda_2) \pm \sqrt{\frac{1}{4}(\lambda_1 - \lambda_2)^2 + \lambda_5^2}, \quad (2.4c)$$

$$e_1 = (\lambda_3 + 2\lambda_4 - 3\lambda_5), \quad (2.4d)$$

$$e_2 = (\lambda_3 - \lambda_5), \quad (2.4e)$$

$$f_1 = f_2 = (\lambda_3 + \lambda_4), \quad (2.4f)$$

$$f_+ = (\lambda_3 + 2\lambda_4 + 3\lambda_5), \quad (2.4g)$$

$$f_- = (\lambda_3 + \lambda_5). \quad (2.4h)$$

When the quartic part of the scalar potential preserves CP and \mathbb{Z}_2 symmetries, the aforementioned eigenvalues are discussed in [35, 36, 39].

Demanding high-scale positivity of the 2HDM potential along various directions in the field space leads to the following conditions on the scalar potential [25, 40–42]:

$$\text{vsc1} : \quad \lambda_1 > 0, \quad (2.5a)$$

$$\text{vsc2} : \quad \lambda_2 > 0, \quad (2.5b)$$

$$\text{vsc3} : \quad \lambda_3 + \sqrt{\lambda_1 \lambda_2} > 0, \quad (2.5c)$$

$$\text{vsc4} : \quad \lambda_3 + \lambda_4 - |\lambda_5| + \sqrt{\lambda_1 \lambda_2} > 0. \quad (2.5d)$$

Meeting the above positivity criteria at each scale of evolution effectively rules out deeper vacua at high energy scales.

In addition to the above, the splitting amongst the scalar masses is restricted by invoking the T -parameter constraint. We have used $\Delta T = 0.05 \pm 0.12$ following [43], where ΔT measures departure from the SM contribution. We have filtered all points in our parameter space through the above constraints and retained only those points that negotiate it successfully. Measurement of the rate for $b \rightarrow s\gamma$ leads to $m_{H^+} \geq 480$ GeV in case of the Type-II 2HDM [44, 45]. In case of Type-I, there is no such lower bound. The constraint $m_{H^+} \geq 80$ GeV originating from direct searches however still persists.

3 Type-I 2HDM: Allowed parameter space for stable vacuum

We start by completing the existing studies [23, 24, 46, 47] on the parameter space allowing for high scale vacuum stability and perturbativity for a Type I 2HDM. A corresponding discussion for the Type-II 2HDM can be seen in [23]. We fix $m_h = 125$ GeV and $M_t = 175$ GeV, the rest of the parameters are generated randomly in the following ranges.

$\tan\beta \in [1, 20]$, $m_H \in [200, 1000]$, $m_A \in [200, 1000]$, $m_{H^+} \in [200, 1000]$, $\cos(\beta - \alpha) \in [-0.4, 0.4]$, $\lambda_6 \in [-1, 1]$, $\lambda_7 \in [-1, 1]$. The generated values of the masses and mixing angles are translated to the basis of the quartic couplings using Eqs. 2.3a to 2.3e.

The strong correlation among the masses, namely $m_H \simeq m_A \simeq m_{H^+}$, is revealed from Fig. 1. This itself can be traced back to Eqs. 2.3a to 2.3e. Any large mass gap results in giving large values for λ_i at the EWSB scale itself, such that they turn non-perturbative rather early in the course of evolution. This feature is also corroborated in [24]. It is important to note that the mass-splitting depends, albeit weakly, on the chosen value of $\tan\beta$. For instance, in case of $\tan\beta = 2$, the maximum splitting allowed is $\simeq 15$ GeV for $\Lambda = 10^{19}$ GeV. This goes down to $\simeq 10$ GeV in case of $\tan\beta = 10$ for the same value of Λ . It should be noted here that the bound on mass splitting that comes from the requirement of perturbativity till high scales is much more stringent than what is obtained by the imposition of the T -parameter constraint alone.

Also important is the ensuing constraint on $\cos(\beta - \alpha)$ which decides the interaction strengths between W, Z and the non-standard scalars. The more suppressed is $\cos(\beta - \alpha)$, closer are the h -interactions to the corresponding values. Thus, measurement of signal strengths of h leads to constraint on this parameter [48–50]. Models valid up to 10^{19} GeV could allow for $|\cos(\beta - \alpha)| \leq 0.15$ and $|\cos(\beta - \alpha)| \leq 0.05$ for $\tan\beta = 2$ and $\tan\beta = 10$ respectively. This bound can be amply relaxed by choosing a lower Λ , for example one finds $|\cos(\beta - \alpha)| \leq 0.14$ in case of $\tan\beta = 10$ if one demands validity up to 10^{19} GeV. This apparent correlation between the UV cut-off scale and the maximum allowed value of $\cos(\beta - \alpha)$, could lead us to predict the maximal extrapolation scale up to which such a 2HDM could be probed at the colliders. Of course, such a

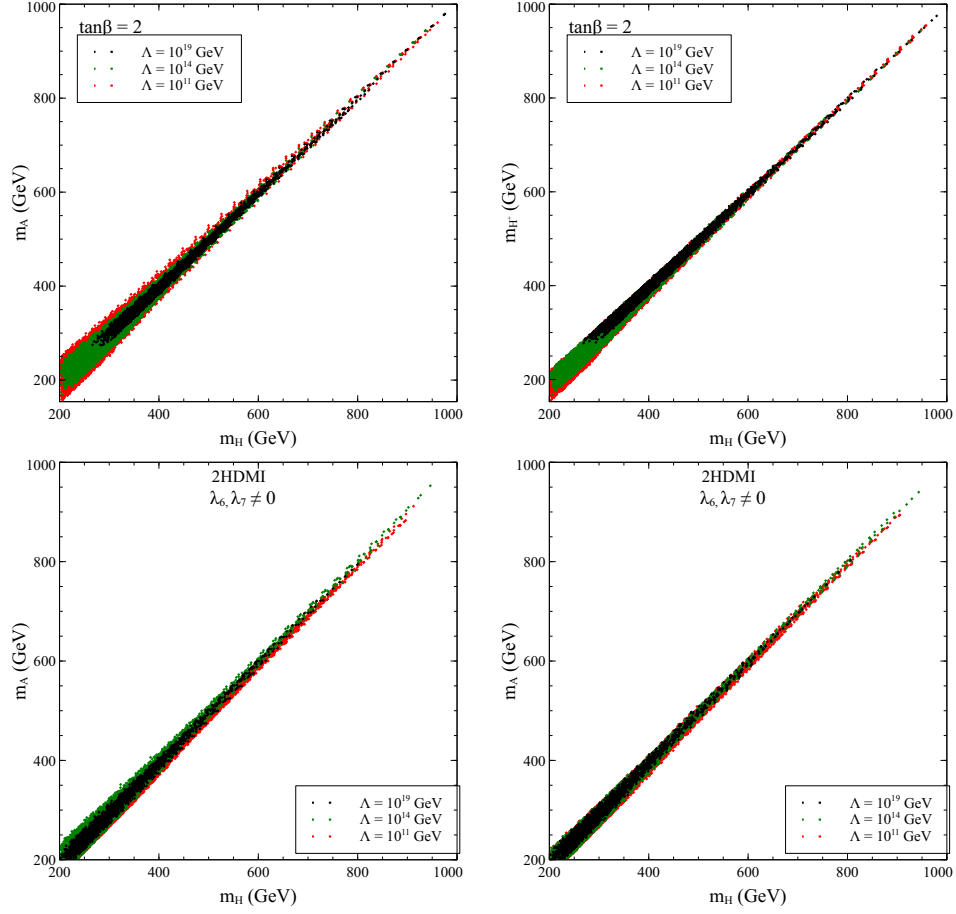


Figure 1: Distribution of the parameter points valid till Λ in the $m_H - m_A$ (left) and $m_H - m_{H^+}$ (right) planes for the Type-I 2HDM. The colour coding can be read from the legends. We fix $\tan\beta = 2$ as a benchmark. The upper(lower) plots correspond to $\lambda_6 = \lambda_7 = 0(\lambda_6, \lambda_7 \neq 0)$. We have varied λ_6, λ_7 in the interval $[-1, 1]$ for the lower plots.

correlation can be noticed for the Type-II scenario as well. The additional result presented here, over and above what is found in the literature, is the establishment of the mass correlations for $\lambda_6, \lambda_7 \neq 0$, as shown in Fig.1.

4 Signals at the LHC: Types I and II.

The previous section illustrates that higher the UV cutoff of a 2HDM is, tighter become the mass-splitting and the bound on $|\cos(\beta - \alpha)|$. Such a constrained scenario makes its observability at the LHC a rather challenging task, as also emphasized in section 1. In particular, if we probe H and A via their decays into reconstructible final states, then the invariant mass distributions of the decay products would coincide. However, probing H and A in reconstructible but distinct final states could enable one to tag the CP of the decaying boson. Given that, we propose the following signals:

- (i) $pp \rightarrow H \rightarrow ZZ \rightarrow 4l$
- (ii) $pp \rightarrow A \rightarrow hZ \rightarrow l^+l^-bb$

We have implemented the model using **FeynRules** [51]. The generated Universal FeynRules Output (UFO) files are then fed to the Monte-Carlo (MC) event generator MadGraph [52] for generation of event samples. The parton-showering and hadronisation is carried out in the PYTHIA-6 [53] framework. We simulated H and A production through the gluon-gluon fusion (ggF) channel using the CTEQ6L1 parton distribution functions. This is because ggF offers higher rates compared to other channels. The renormalisation and factorisation scales have been set at m_H and m_A for the first and second signals respectively. We mention in this context that detector simulation and analysis of the events were done using **Delphes** [54].

For simulating the proposed final states, we hold m_H and m_A fixed and scan over the remaining input quantities. From the randomly generated parameter sets, we select an illustrative assortment of benchmark points (Table 1) to highlight the main findings of the analysis.

The benchmarks are distinct from another *vis-a-vis* RG evolution patterns. While choosing them, it was ensured that the UV-cutoff of a given benchmark does not change upon switching between the Type-I and Type-II models. For instance, in the case where $\lambda_6 = \lambda_7 = 0$, BP1b, BP1b, BP3c, BP4c and BP5c are conservative input sets ensuring a stable vacuum and a perturbative model till $\sim 10^{19}$ GeV. This can be read from the small values of $|\cos(\beta - \alpha)|$ characterizing them. The other benchmarks are however not that conservative, but still they manage to stabilise the vacuum till at least 10^{11} GeV. Likewise, BP3b and BP4b are included to estimate the statistical significance of scenarios valid till 10^{14} GeV. For a given set of couplings, elevating the masses of H and A progressively diminishes the intensity of the signals, and, also narrows the allowed band of $|\cos(\beta - \alpha)|$. The choice of the benchmarks is thus guided by the aim to understand the maximum m_H, m_A as well as the highest UV cut-off up to which the scenario can be experimentally observed.

4.0.1 $pp \rightarrow H \rightarrow ZZ \rightarrow 4l$

H_2 is produced through gluon fusion and decays to two on-shell Z bosons. We look for a final state where the Z bosons subsequently decay into four leptons [55]. The dominant background for this process comes from $ZZ(^*)$ production. Taking into account subleading contributions from the $Z\gamma$ and $\gamma\gamma$ channels and

Benchmark	$m_H(\text{GeV})$	$m_A(\text{GeV})$	$m_{12}(\text{GeV})$	$\cos(\beta - \alpha)$
BP1a	350	351	200	-0.18
BP1b	350	351	200	-0.12
BP2a	400	401	230	-0.15
BP2b	400	401	230	-0.10
BP3a	500	501	280	-0.095
BP3b	500	501	280	-0.070
BP3c	500	501	280	-0.050
BP4a	550	551	320	-0.075
BP4b	550	551	320	-0.060
BP4c	550	551	320	-0.050
BP5a	600	601	350	-0.050
BP5b	600	601	350	-0.035
BP5c	600	601	350	-0.025

Table 1: Benchmarks chosen for simulating the proposed channels. We have taken $m_h = 125$ GeV and $\tan\beta = 2.5$ throughout. Any higher $\tan\beta$ would to a lower ggF rate and so was not chosen.

multiplying by appropriate next-to-leading order (NLO) K-factors [52], the total background cross section is $\simeq 42$ fb. Some basic cuts, as listed below, were applied during event generation.

Basic-cuts:

- All leptons have a minimum transverse momentum of 10 GeV, $p_T^l \geq 10$ GeV.
- Pseudorapidity of the leptons must lie within the window $|\eta^l| \leq 2.5$.
- All possible lepton-pairs are resolved using $\Delta R_{ll} > 0.3$.

We multiply the ggF cross sections of H production by an NLO K factor of 1.5. The cuts listed below were further imposed.

Selection cuts:

- **SC1:** The invariant mass of the final state leptons lie within the window $m_H - 15 \text{ GeV} \leq m_{4l} \leq m_H + 15 \text{ GeV}$.
- **SC2:** The transverse momenta of the leptons lie above the thresholds $p_T^{l_1} > p_{T,\min}^{l_1}$, $p_T^{l_2} > p_{T,\min}^{l_2}$, $p_T^{l_3} > 30 \text{ GeV}$, $p_T^{l_4} > 20 \text{ GeV}$.
- **SC3:** Transverse momenta of the reconstructed Z -bosons satisfy $p_T^{Z_1} > p_{T,\min}^{Z_1}$, $p_T^{Z_2} > p_{T,\min}^{Z_2}$.

We take $p_T^{Z_1/Z_2} = 20, 20, 40, 50, 70 \text{ GeV}$ and $\{p_{T,\min}^{l_1}, p_{T,\min}^{l_2}\} = \{50 \text{ GeV}, 30 \text{ GeV}\}, \{50 \text{ GeV}, 30 \text{ GeV}\}, \{80 \text{ GeV}, 50 \text{ GeV}\}, \{90 \text{ GeV}, 70 \text{ GeV}\}, \{100 \text{ GeV}, 70 \text{ GeV}\}$ for BP1, BP2, BP3, BP4, BP5 respectively, the decisive factor in this choice of $p_T^{Z_1/Z_2}$ being m_H , for any benchmark point.

For $m_H > 500$ GeV, the leading and the subleading leptons are strongly boosted, thus having a good probability of surviving the strong p_T cuts. In addition, appropriate cuts on the p_T of the Z-bosons also contributes towards improving the signal-to-background ratio. Denoting the number of signal and background events as \mathcal{N}_S and \mathcal{N}_B at a given integrated luminosity (\mathcal{L}), the statistical significance or the confidence limit (CL) is defined as $\text{CL} = \frac{\mathcal{N}_S}{\sqrt{\mathcal{N}_S + \mathcal{N}_B}}$.

Benchmark	σ_S^{SC} (fb)	σ_B^{SC} (fb)	\mathcal{N}_S^{100}	\mathcal{N}_B^{100}	\mathcal{N}_S^{3000}	\mathcal{N}_B^{3000}	CL ₁₀₀	CL ₃₀₀₀
BP1a	0.173	0.334	17.36	33.40	520.94	1002.18	2.43	13.34
BP1b	0.145	0.334	14.54	33.40	436.31	1002.18	2.10	11.503
BP2a	0.104	0.194	10.42	19.46	312.73	584.00	1.90	10.44
BP2b	0.071	0.194	7.11	19.46	213.38	584.00	1.37	7.55
BP3a	0.026	0.064	2.59	6.48	77.99	194.60	0.86	4.72
BP3b	0.016	0.064	1.68	6.48	50.52	194.60	0.58	3.22
BP3c	0.009	0.064	0.97	6.48	29.37	194.60	0.35	1.96
BP4a	0.011	0.041	1.13	4.16	34.06	124.91	0.49	2.70
BP4b	0.008	0.041	0.81	4.16	24.52	124.91	0.36	2.00
BP4c	0.006	0.041	0.61	4.16	18.33	124.91	0.27	1.53
BP5a	0.004	0.029	0.41	2.96	12.32	89.090347	0.22	1.22
BP5b	0.002	0.029	0.22	2.96	6.70	89.090347	0.12	0.68
BP5c	0.001	0.029	0.12	2.96	3.61	89.090347	0.06	0.37

Table 2: A record of the number of surviving events in the $H \rightarrow 4l$ channel after the selection cuts at the $\sqrt{s} = 14$ TeV LHC for a Type-I 2HDM. Here $\mathcal{N}_S^{100(3000)}$ and $\mathcal{N}_B^{100(3000)}$ and respectively denote the number of events $\mathcal{L} = 100(3000) \text{ fb}^{-1}$. Besides, $\text{CL}_{100(3000)}$ denotes the confidence level at $\mathcal{L} = 100(3000) \text{ fb}^{-1}$.

Tables 2 and 3 contain the estimated CL for all the benchmarks. The following features thus emerge:

- (i) The statistical significance diminishes as m_H is increased. This is due to two reasons. First, the ggF cross section for a single H drops. Secondly, the higher is m_H , the smaller is the upper limit on $|\cos(\beta - \alpha)|$ consistent with high scale stability, and hence, the lower is the $H \rightarrow ZZ$ branching ratio.
- (ii) Type-I 2HDM offers a marginally higher significance as compared with Type-II. This is entirely attributed to the persistence of a slightly higher $H \rightarrow ZZ$ branching ratio in Type-I.
- (iii) For $m_H \simeq 350$ GeV, an integrated luminosity of 100 fb^{-1} is sufficient to yield a 3σ significance.
- (iv) To observe an H of mass around $\simeq 500$ GeV that originates from a 2HDM valid till 10^{19} GeV with a minimum of 3σ confidence level, one needs to gather 3000 fb^{-1} of data at the LHC. The statistical significance decreases for higher masses. In short, the observability of a given H can be improved by either lowering m_H and holding the UV cutoff fixed or vice versa. This interplay is illustrated in Fig. 2 and Fig. 3.

Fig. 2 corroborates the previous observation that an H with $m_H = 500$ GeV can lead to a 3σ signal at the LHC, consistently with perturbativity as well as a stable vacuum till 10^{19} GeV. This is true for both Type-I and Type-II 2HDM. Note that the parameter space relaxes upon the introduction of non-vanishing λ_6 and λ_7 . This marginally helps in elevating the UV cutoff without compromising on the strength of the signal.

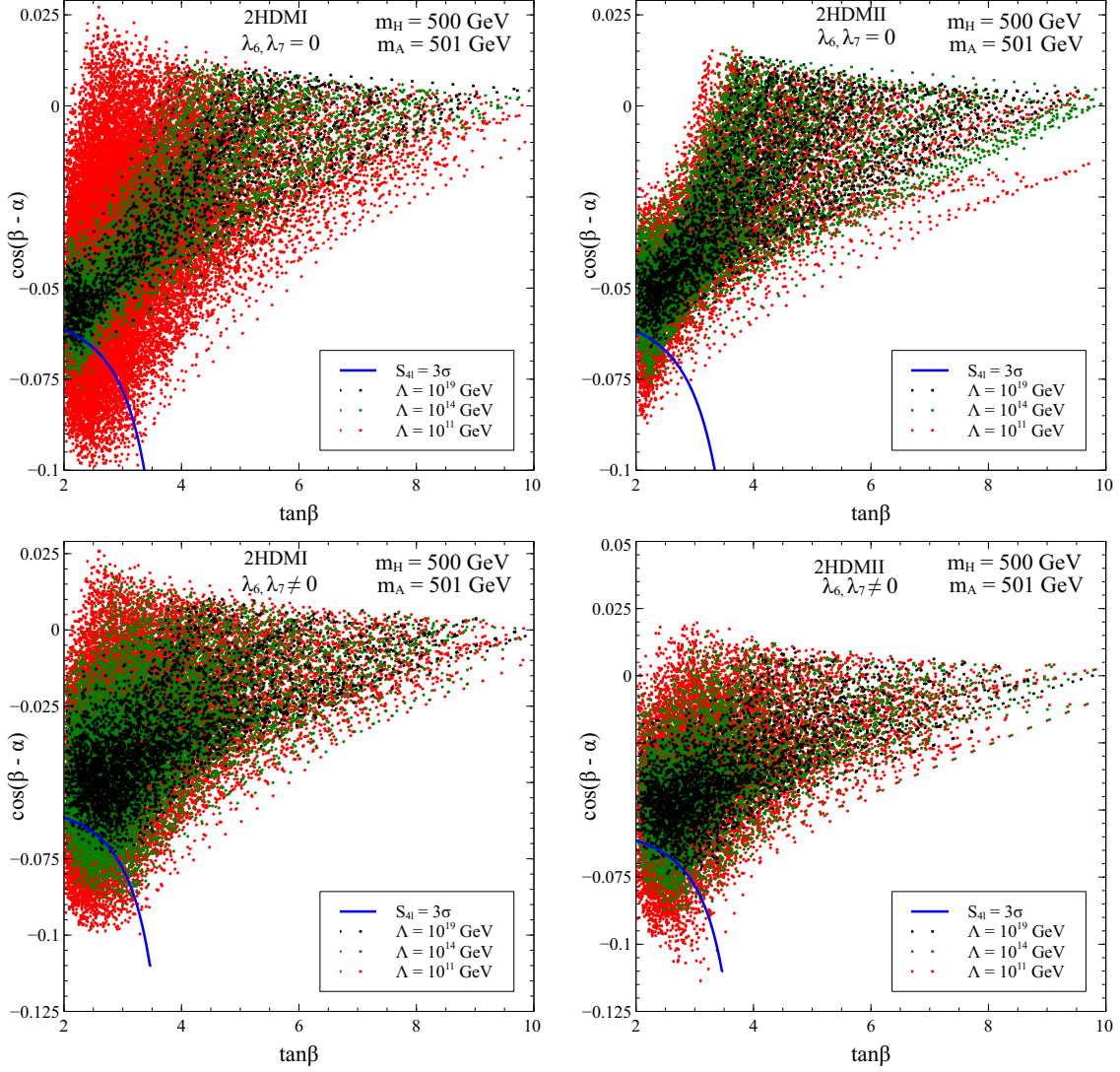


Figure 2: The parameter space in the $\tan\beta$ vs. $\cos(\beta - \alpha)$ plane for $m_H = 500$ GeV and $m_A = 501$ GeV that allows for validity till 10^{11} GeV (red), 10^{14} GeV (green) and 10^{19} GeV (black). The region inside the blue curve corresponds to a signal significance greater than or equal to 3σ . The upper and lower plots are for $\lambda_6 = \lambda_7 = 0$ and $\lambda_6, \lambda_7 \neq 0$ respectively.

Benchmark	σ_S^{SC} (fb)	σ_B^{SC} (fb)	\mathcal{N}_S^{100}	\mathcal{N}_B^{100}	\mathcal{N}_S^{3000}	\mathcal{N}_B^{3000}	CL ₁₀₀	CL ₃₀₀₀
BP3a	0.025	0.064	2.56	6.48	76.99	194.60	0.85	4.67
BP3b	0.016	0.064	1.65	6.48	49.65	194.60	0.58	3.17
BP3c	0.009	0.064	0.95	6.48	28.73	194.60	0.35	1.92
BP4a	0.011	0.041	1.12	4.16	33.64	124.91	0.48	2.67
BP4b	0.008	0.041	0.80	4.16	24.15	124.91	0.36	1.97
BP4c	0.006	0.041	0.60	4.16	18.02	124.91	0.27	1.50
BP5a	0.004	0.029	0.40	2.96	12.148	89.09	0.22	1.20
BP5b	0.002	0.029	0.21	2.96	6.58	89.09	0.124	0.67
BP5c	0.001	0.029	0.11	2.96	3.54	89.09	0.06	0.36

Table 3: A record of the number of surviving events in the $H \rightarrow 4l$ channel after the selection cuts at the $\sqrt{s} = 14$ TeV LHC for a Type-II 2HDM. Here $\mathcal{N}_S^{100(3000)}$ and $\mathcal{N}_B^{100(3000)}$ and respectively denote the number of events $\mathcal{L} = 100(3000) \text{ fb}^{-1}$. Besides, CL₁₀₀₍₃₀₀₀₎ denotes the confidence level at $\mathcal{L} = 100(3000) \text{ fb}^{-1}$.

For $m_H = 550$ GeV, on the other hand, a 2HDM (of either Type-I or Type-II) cannot be extrapolated beyond 10^{11} GeV if a 3σ statistical significance has to be maintained. This is confirmed by an inspection of Fig. 3.

We examine the prospects of reconstructing A through the proposed $l^+l^-b\bar{b}$ final state in the following section.

4.0.2 $pp \rightarrow A \rightarrow hZ \rightarrow l^+l^-b\bar{b}$

In the absence of CP-violation (as assumed here), the hZ pair production points towards a CP-odd parent particle [56], and a peak in the invariant mass close to the afore mentioned ZZ peak should be the smoking gun signal of the near degeneracy of a scalar and a pseudoscalar. However, $pp \rightarrow t\bar{t}$ generates the dominant background for this final state. Subleading contributions come from the production of ZWW and $Zb\bar{b}$. Similar to the previous analysis, we adopt a K -factor = 1.5 for pseudoscalar production for all the benchmarks. The following cuts are applied during event-generation.

Basic cuts:

- $p_T^l \geq 10 \text{ GeV}$, $p_T^b \geq 20 \text{ GeV}$
- $|\eta^l| \leq 2.5$, $|\eta^b| \leq 2.5$
- $\Delta R_{ll} > 0.3$, $\Delta R_{lb} > 0.4$, $\Delta R_{bb} > 0.4$

On applying the above cuts, the NLO background cross section turns out to be $\simeq 32 \text{ pb}$. The following cuts are imposed for an efficient background rejection.

Selection cuts:

- C1: The invariant mass of the leptons satisfy $85.0 \text{ GeV} \leq m_{ll} \leq 100 \text{ GeV}$.

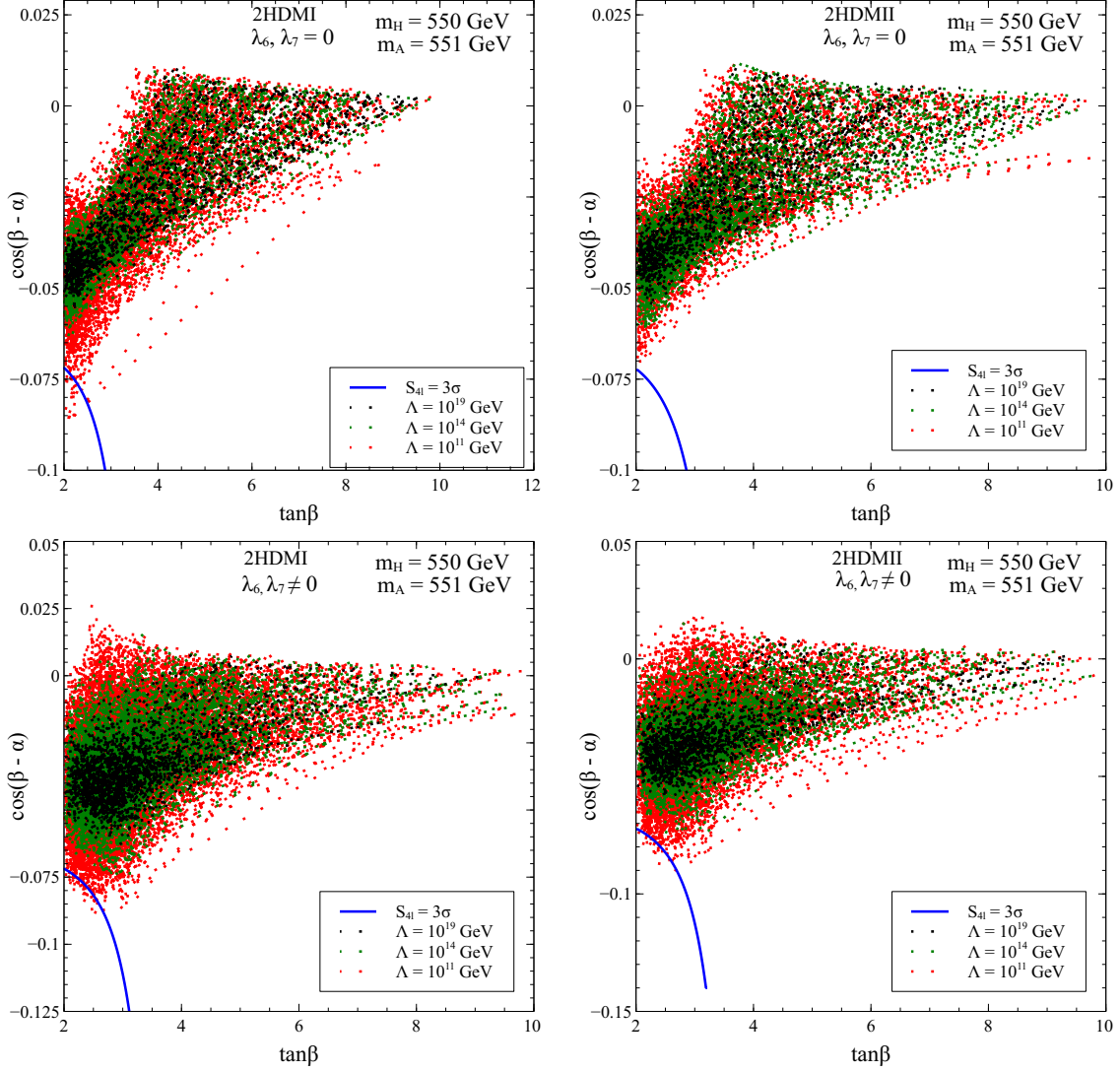


Figure 3: The parameter space in the $\tan\beta$ vs. $\cos(\beta - \alpha)$ plane for $m_H = 550$ GeV and $m_A = 551$ GeV that allows for validity till 10^{11} GeV (red), 10^{14} GeV (green) and 10^{19} GeV (black). The region inside the blue curve corresponds to a signal significance greater than or equal to 3σ . The upper and lower plots are for $\lambda_6 = \lambda_7 = 0$ and $\lambda_6, \lambda_7 \neq 0$ respectively.

- C2: The invariant mass of the b-jets satisfy $95.0 \text{ GeV} \leq m_{bb} \leq 155 \text{ GeV}$.
- C3: The scalar sum of the transverse momenta of the leptons and b-jets satisfies $\sum_{l,b} p_T > (\sum_{l,b} p_T)_{\min}$.
- C4: An upper bound on the missing transverse momenta, $\cancel{E}_T \leq 30 \text{ GeV}$.
- C5: The invariant mass of the $2l - 2b$ system lies within the range $m_A - 30 \text{ GeV} \leq m_{llbb} \leq m_A + 30 \text{ GeV}$.
- C6: p_T of the reconstructed Z -boson satisfies $p_T^Z > 120 \text{ GeV}$ for BP5, and,
 $> 100 \text{ GeV}$ for the rest
- C7: Upper bounds on the p_T of the b-jets, $p_T^{b_1} > p_{T,\min}^{b_1}$.

The cuts on the p_T of leading b-jet as well as on scalar the sum of the p_T of the b-jets and leptons are appropriately strengthened with increase in m_A . We opt for $\{(\sum_{l,b} p_T)_{\min}, p_T^{b_1}\} = \{270 \text{ GeV}, 40 \text{ GeV}\}$ for BP1, $\{320 \text{ GeV}, 40 \text{ GeV}\}$ for BP2, $\{350 \text{ GeV}, 50 \text{ GeV}\}$ for BP3 and BP4, and, $\{380 \text{ GeV}, 70 \text{ GeV}\}$ for BP5. The selection cuts involve reconstructing the invariant masses of not only the decaying A , but also of the Z and the h , appropriately in each case. A lower limit on the scalar sum of the p_T of the leptons and the b -hadrons also aids in increasing the significance. All the \cancel{E}_T in the signal is generated from mis-measurement of the momenta of the visible particles, thus generating a soft missing \cancel{E}_T distribution. On the other hand, the corresponding background has a harder p_T spectrum since the $t\bar{t}$ and ZWW channels always lead to neutrinos in the final state. Therefore, a suitable upper bound on the missing transverse energy reduces a portion of these backgrounds.

In this channel, too, Type-I fares slightly better than Type-II, much due to the same reason outlined in preceding discussion. In this channel, The statistical significance of BP1-5 is also enhanced *w.r.t* the $4l$ case, albeit marginally. The confidence level corresponding to $m_A = 500 \text{ GeV}$ looms around 3σ , for both Type-I and Type-II.

A clearer picture regarding the observability of an A of masses 500 GeV and 550 GeV emerge upon inspection of Fig. 4 and Fig. 5 respectively. We display the 5σ contour as well in case of the $l^+l^-b\bar{b}$ channel. For $m_A = 550 \text{ GeV}$ with non-zero λ_6 and λ_7 , the $l^+l^-b\bar{b}$ channel offers sensitivity at the level of 3σ for a scenario valid till 10^{14} GeV or even higher. On the contrary, the corresponding cut-off cannot be pushed above 10^{11} GeV if one demands similar observability in case of the $4l$ final state from H -decay. Overall, a violation of the Z_2 symmetry via λ_6 and λ_7 aids to the effort of observing a 2HDM valid up to high cut-off scales.

It is mentioned that the analysis for this channel is subject to uncertainties, albeit small, that are introduced while estimating the background cross section. Upon considering the errors in the $t\bar{t}$ production rates and the background NLO K-factors [52], the total background cross section can deviate up to $\simeq \pm 20\%$. This, however, does not modify the overall conclusions made in this section.

5 Prospects at other colliders

With the prospects of observing non-standard scalars with masses above the 500 GeV range at the LHC turning bleak, we resort to future lepton colliders for better observability. These include not only the e^+e^- colliders, but also a muon collider [22].

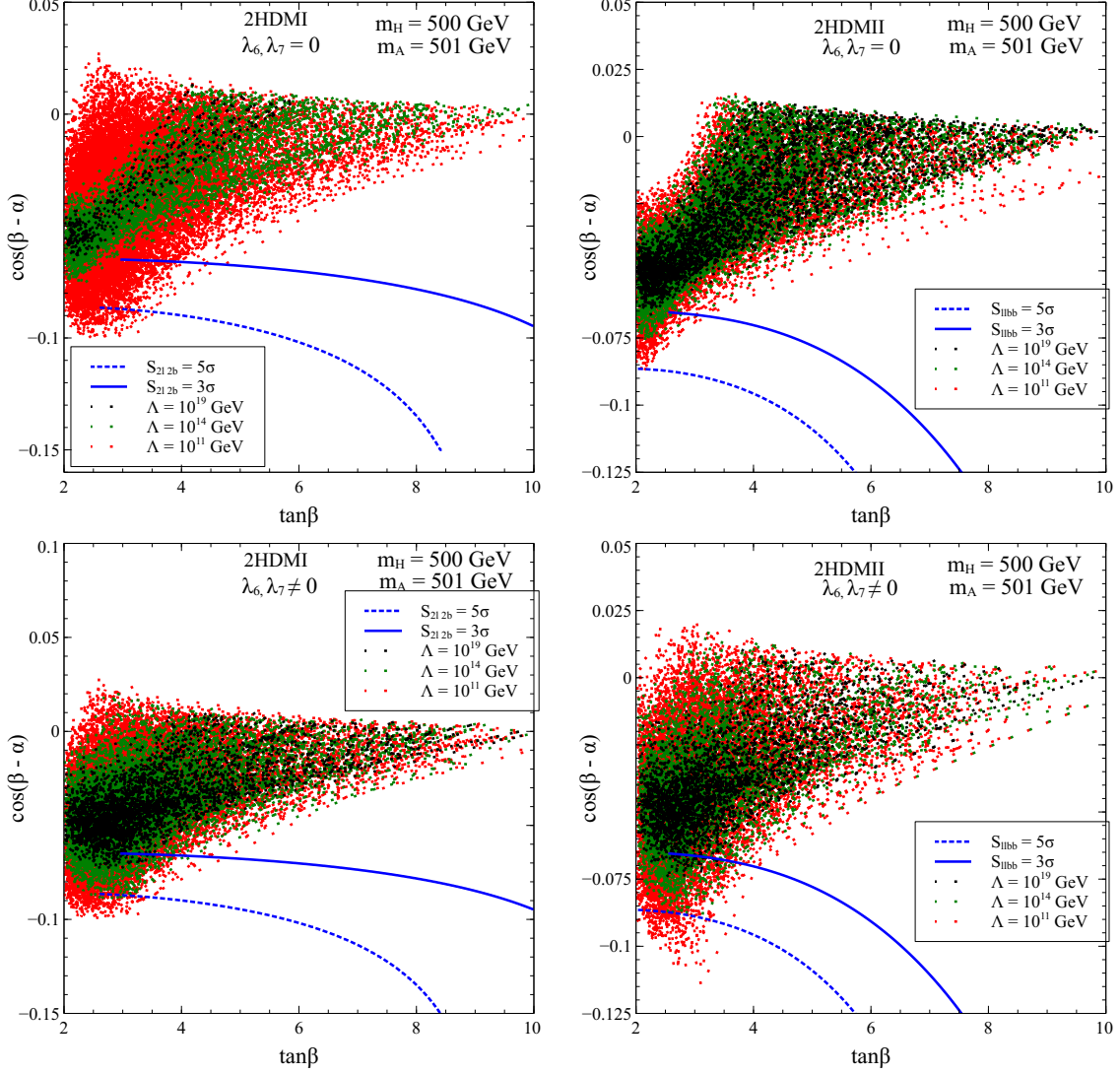


Figure 4: The parameter space in the $\tan\beta$ vs. $\cos(\beta - \alpha)$ plane for $m_H = 500$ GeV and $m_A = 501$ GeV that allows for validity till 10¹¹ GeV (red), 10¹⁴ GeV (green) and 10¹⁹ GeV (black). The region inside the solid (broken) blue curve corresponds to a signal significance greater than or equal to 3(5) σ . The upper and lower plots are for $\lambda_6 = \lambda_7 = 0$ and $\lambda_6, \lambda_7 \neq 0$ respectively.

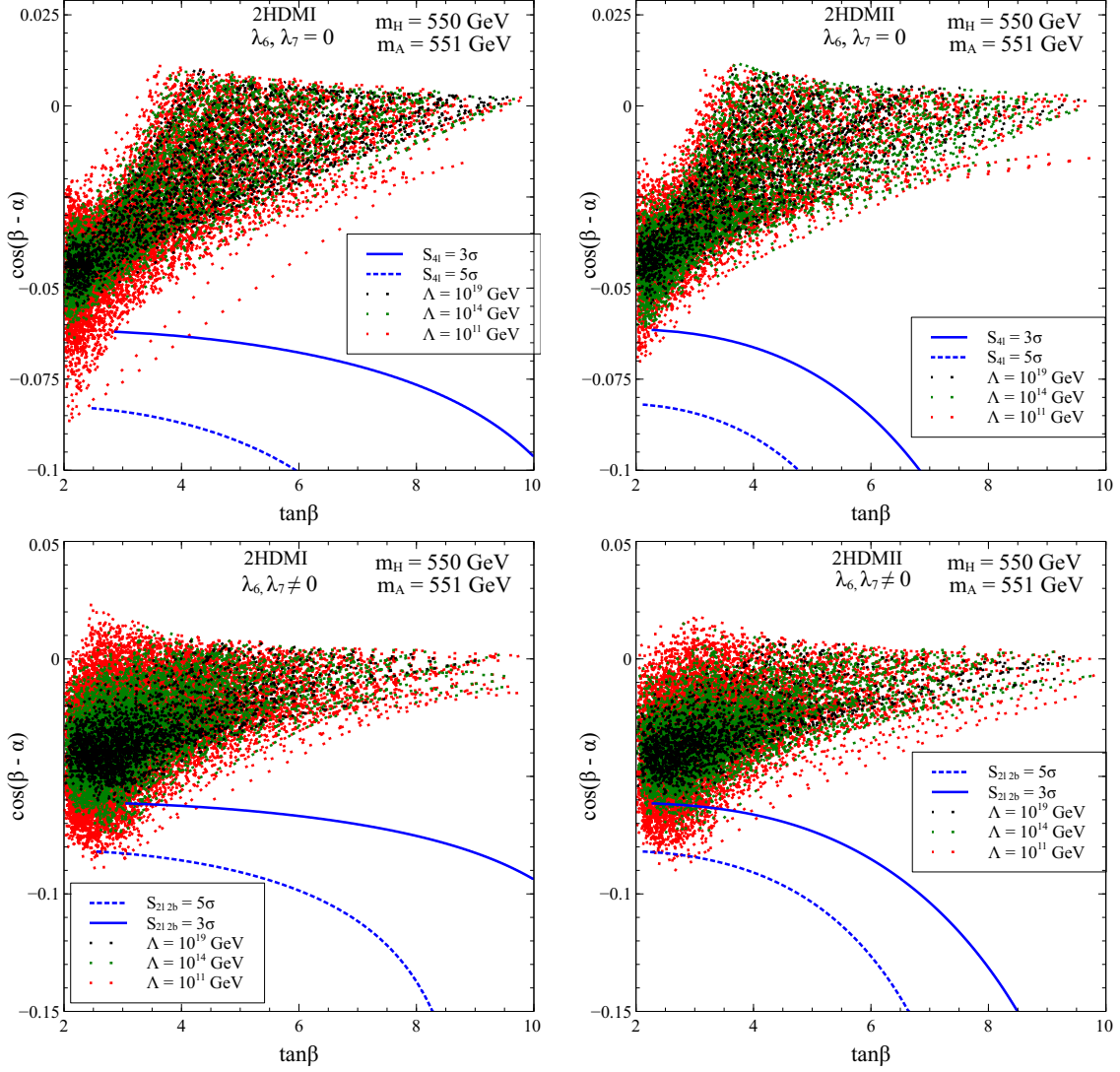


Figure 5: The parameter space in the $\tan\beta$ vs. $\cos(\beta - \alpha)$ plane for $m_H = 550$ GeV and $m_A = 551$ GeV that allows for validity till 10^{11} GeV (red), 10^{14} GeV (green) and 10^{19} GeV (black). The region inside the solid (broken) blue curve corresponds to a signal significance greater than or equal to $3(5)\sigma$. The upper and lower plots are for $\lambda_6 = \lambda_7 = 0$ and $\lambda_6, \lambda_7 \neq 0$ respectively.

Benchmark	σ_S^{SC} (fb)	σ_B^{SC} (fb)	\mathcal{N}_S^{300}	\mathcal{N}_B^{100}	\mathcal{N}_S^{3000}	\mathcal{N}_B^{3000}	CL ₁₀₀	CL ₃₀₀₀
BP1a	1.65	10.94	164.60	1094.05	4938.02	32821.48	4.64	25.41
BP1b	0.90	10.94	89.55	1094.05	2686.45	32821.48	2.60	14.26
BP2a	0.55	4.30	55.22	430.24	1656.63	12907.32	2.51	13.73
BP2b	0.28	4.30	27.92	430.24	837.64	12907.32	1.30	7.14
BP3a	0.132	1.387	13.24	138.73	397.11	4161.95	1.07	5.88
BP3b	0.076	1.387	7.63	138.73	228.91	4161.95	0.63	3.45
BP3c	0.041	1.387	4.05	138.73	121.52	4161.95	0.34	1.86
BP4a	0.066	0.632	6.56	63.22	196.86	1896.59	0.79	4.30
BP4b	0.044	0.632	4.35	63.22	130.50	1896.59	0.53	2.90
BP4c	0.031	0.632	3.08	63.22	92.53	1896.59	0.38	2.07
BP5a	0.021	0.334	2.07	33.37	62.19	1000.98	0.35	1.91
BP5b	0.010	0.334	1.05	33.37	31.38	1000.98	0.18	0.98
BP5c	0.005	0.334	0.54	33.37	16.27	1000.98	0.09	0.51

Table 4: A record of the number of surviving events in the $A \rightarrow l^+ l^- b \bar{b}$ channel after the selection cuts at the $\sqrt{s} = 14$ TeV LHC for a Type-I 2HDM. Here $\mathcal{N}_S^{100(3000)}$ and $\mathcal{N}_B^{100(3000)}$ and respectively denote the number of events with $\mathcal{L} = 100(3000) \text{ fb}^{-1}$. Besides, CL₁₀₀₍₃₀₀₀₎ denotes the confidence level for $\mathcal{L} = 100(3000) \text{ fb}^{-1}$.

The principal heavy Higgs production channels at the e^+e^- machine are those of associated production (VH) and Vector-Boson-Fusion (VBF) [57]. The production rate in both of these modes is controlled by the value of $\cos(\beta - \alpha)$. As elaborated in the previous sections, $\cos(\beta - \alpha)$ is tightly bounded by the requirement of a stable vacuum till the Planck scale. In addition, the maximum \sqrt{s} proposed for the ILC is 1 TeV [58] which hampers a probe of heavy scalars due to kinematical limitations. For instance, the VH production cross section for an H of mass 600 GeV could be at most $\simeq 0.01 \text{ fb}$ in a ILC with $\sqrt{s} = 1 \text{ TeV}$. This does not result in the requisite signal significance when the backgrounds are estimated and the cut efficiencies are folded in.

5.1 $\mu^+ \mu^-$ collisions and radiative return

A particularly interesting process in a muon collider is one of radiative return (RR) [59], where one does not need to know the mass of the resonantly produced scalar precisely. In our context, the processes under consideration are

$$\mu^+ \mu^- \longrightarrow H \gamma, A \gamma \quad (5.1)$$

Note here that H/A can be produced in association with a γ in t-channel $\mu^+ \mu^-$ annihilations. When the center of mass energy of the muon collider is above the heavy resonance, the photon emission from the initial state provides an opportunity to reconstruct the mass of the heavy scalar or pseudoscalar. For this, one need not know the mass of the (unknown) heavy resonance. The final state then consists of a soft photon

Benchmark	σ_S^{SC} (fb)	σ_B^{SC} (fb)	\mathcal{N}_S^{300}	\mathcal{N}_B^{100}	\mathcal{N}_S^{3000}	\mathcal{N}_B^{3000}	CL ₁₀₀	CL ₃₀₀₀
BP3a	0.130	1.387	13.01	138.73	390.23	4161.95	1.06	5.78
BP3b	0.075	1.387	7.49	138.73	224.80	4161.95	0.62	3.39
BP3c	0.040	1.387	3.98	138.73	119.30	4161.95	0.33	1.82
BP4a	0.065	0.632	6.45	63.22	193.61	1896.59	0.77	4.23
BP4b	0.043	0.632	4.28	63.22	128.30	1896.59	0.52	2.85
BP4c	0.030	0.632	3.03	63.22	90.95	1896.59	0.37	2.04
BP5a	0.020	0.334	2.04	33.37	61.18	1000.98	0.34	1.88
BP5b	0.010	0.334	1.03	33.37	30.87	1000.98	0.18	0.96
BP5c	0.005	0.334	0.53	33.37	16.00	1000.98	0.09	0.50

Table 5: A record of the number of surviving events in the $A \rightarrow l^+ l^- b \bar{b}$ channel after the selection cuts at the $\sqrt{s} = 14$ TeV LHC for a Type-II 2HDM. Here $\mathcal{N}_S^{100(3000)}$ and $\mathcal{N}_B^{100(3000)}$ and respectively denote the number of events with $\mathcal{L} = 100(3000) \text{ fb}^{-1}$. Besides, CL₁₀₀₍₃₀₀₀₎ denotes the confidence level at for $\mathcal{L} = 100(3000) \text{ fb}^{-1}$.

and other visible products exhibiting an invariant mass peak. The closer is the mass of the heavy scalar to the centre-of-mass (COM) energy of $\mu^+ \mu^-$ collisions, the higher the cross section.

Thus tagging a heavy scalar state from invariant mass peak of its decay product can help us in reducing the background and increasing the statistical significance. Moreover, in order to obtain information on the CP of the heavy resonance, the CP-even and the CP-odd states must be allowed to decay in different final states following their production through RR. We can propose $H \rightarrow ZZ \rightarrow 4l$ and $A \rightarrow hZ \rightarrow l^+ l^- b \bar{b}$, which resemble the signals studied in the previous sections, and distinguish the cP-even scalar from the CP-odd one. In order to study the observability of the benchmarks BP3a - BP5c in RR, we choose the COM energy of the $\mu^+ \mu^-$ collisions to be just 10 GeV above m_H , in each case. For BP3a, the RR cross section for H production is $\simeq 1.3 \text{ fb}$ for a Type-II 2HDM. Upon multiplying by the branching ratios corresponding to $H \rightarrow ZZ$ and $Z \rightarrow ll$, the corresponding cross section for the $4l + \gamma$ final state turns out to be $\mathcal{O}(10^{-4}) \text{ (fb)}$. The cross section for the $l^+ l^- b \bar{b} + \gamma$ final state could still be $\mathcal{O}(10^{-3}) \text{ (fb)}$. However, it will ultimately get reduced when kinematical cuts are applied. In a Type-II 2HDM, though the $\mu\mu H$ coupling is proportional to $\tan\beta$, opting for a higher value of $\tan\beta$ does not help in this regard, since in that case, the allowed value of $|\cos(\beta - \alpha)|$ decreases owing to the demand of validity till high scales (see Fig.). This diminishes the $H \rightarrow ZZ$ and $A \rightarrow hZ$ branching ratios, and ultimately, leads to further lower rates. The other BPs too predict negligibly small RR rates for both Type-I and Type-II. With such meagre RR rates in $4l + \gamma$ as well as $l^+ l^- b \bar{b} + \gamma$ channels, chances of observing the heavy resonances are obliterated.

Still promising could the fermionic decay channels of H/A in this regard. For instance, the $b \bar{b} A$ coupling in a Type-(I)II 2HDM is proportional to $\cot\beta(\tan\beta)$ and for sufficiently small $|\cos(\beta - \alpha)|$, the fermionic couplings of H and A are nearly equal. The advantage of a muon collider over the LHC is that the $b \bar{b}$ final state can rise above the background more effectively. As we shall see below, this enhances the mass reach.

One can thus probe the observability of the heavy scalars in the $\mu^+\mu^- \rightarrow H/A\gamma \rightarrow b\bar{b}\gamma$ ². It is readily seen that for $\tan\beta > 1$, Type-II has higher production rates of H/A through RR compared to Type-I. This could give a handle in distinguishing between Types I and II. Therefore, to test the potency of RR in the $H/A \rightarrow b\bar{b}$ mode, we tabulate two additional benchmarks, as shown in Table 6.

Benchmark	\sqrt{s} (GeV)	$\tan\beta$	m_H (GeV)	m_A (GeV)
BP6	500	12	492	493
BP7	1000	12	992	993

Table 6: The values of m_H , m_A and $\tan\beta$ chosen to probe the radiative return channel. The values of \sqrt{s} are also shown.

The values of the other 2HDM parameters have been fixed appropriately so as to ensure stability till the Planck scale. For instance, we chose $m_{12} = 150$, $c_{\beta-\alpha} = 0.01$ and $m_{12} = 500$, $c_{\beta-\alpha} = 0.005$ for BP6 and BP7 respectively. We take 500 GeV and 1 TeV to be COM energy for these two cases. Accordingly, $\sqrt{s} - m_{H/A}$ is maintained around ~ 7 GeV to maximize the efficiency of the radiative return mechanism. In addition, we have purposefully chosen a somewhat large value for $\tan\beta$ to elevate the H/A production rate to the order of 10 fb. Moreover, we also get a sizeable branching ratio for the $H/A \rightarrow b\bar{b}$ channel for both BP6 and BP7 ($> 70\%$).

The SM background comes from the processes $\mu^+\mu^- \rightarrow b\bar{b}$ and $\mu^+\mu^- \rightarrow b\bar{b}\gamma$. The cut, $m_H - 30 \text{ GeV} < m_{bb} < m_H + 30 \text{ GeV}$ on the invariant mass of the b -pair is imposed. The softness of the photon in the case of RR can be exploited to reduce the background by putting an upper bound on the photon p_T , which we take to be 30 GeV. Effects arising out of smearing the photon-energy are small, so we keep the photon-energy same as the simulated value. The confidence levels obtained for BP6 and BP7 are listed in Table 7.

Benchmark	σ_S^{SC} (fb)	σ_B^{SC} (fb)	\mathcal{N}_S^{500}	\mathcal{N}_B^{500}	\mathcal{N}_S^{1000}	\mathcal{N}_B^{1000}	CL ₅₀₀	CL ₁₀₀₀
BP6	2.02	32.22	1011.28	16110.05	2022.56	32220.08	7.72	10.92
BP7	0.26	2.52	133.92	1264.28	267.85	2528.57	3.58	5.06

Table 7: Number of signal and background surviving events in the radiative return process at the muon collider. Here $\mathcal{N}_S^{500(1000)}$ and $\mathcal{N}_B^{500(1000)}$ and respectively denote the number of events $\mathcal{L} = 500(1000) \text{ fb}^{-1}$. Besides, CL₅₀₀₍₁₀₀₀₎ denotes the confidence level at $\mathcal{L} = 500(1000) \text{ fb}^{-1}$.

Table 7 shows that it is possible to experimentally observe an H as heavy as 1 TeV through radiative return. The corresponding signal rates are almost identical for a near degenerate A decaying to $b\bar{b}$, and thus, are not separately shown. Thus, radiative return in the $b\bar{b}$ channel does succeed in predicting abundant signal events in case of heavy scalars. This is reflected by a sizable statistical significance of $\sim 5\sigma$ that can be obtained in case of a scalar of mass 1 TeV when the $\mu^+\mu^-$ machine is operated at an integrated luminosity of 1000 fb^{-1} . More importantly, this is found to be in perfect agreement with high-scale stability

²In view of the high t -Yukawa coupling, one could also look at $\mu^+\mu^- \rightarrow H/A\gamma \rightarrow t\bar{t}\gamma$ in principle. However that channel will ultimately lead to lesser rates compared to the $b\bar{b}$ mode owing to the smaller $t\bar{t}$ branching fraction.

and perturbativity up to M_{Pl} . However in this channel, one faces the difficulty in distinguishing between a $b\bar{b}$ resonance that comes from an H and one coming from A . This is in sharp contrast with the results obtained in case of the 14 TeV LHC. Over there, though the CP of the scalar can be tagged, its observability does not exceed 3σ in terms of confidence level for masses beyond 500 GeV.

6 Summary and conclusions.

By virtue of the additional bosonic fields, a 2HDM ensures the stability of the EW vacuum till a cut-off scale all the way up to the Planck scale. This holds true even after switching between the Type-I and Type-II cases. However stringent constraints apply on the parameter space in the process. This is especially true when vacuum stability and perturbative unitarity are demanded up to the Planck scale. Then, the couplings of the non-standard scalars to other bosonic states become very small because of suppressed $\cos(\beta - \alpha)$. In addition, the mass spectrum of the non-standard scalar bosons becomes quasi-degenerate. These constraints limit the observability of such a 2HDM at colliders.

We have studied in detail the interplay between high-scale validity and the discernability of the scenario at the LHC and at a future muon collider. In the LHC, signatures of the CP-even boson H and CP-odd boson A are studied through their decays into the $4l$ and $l^+l^-b\bar{b}$ channel respectively. The search turns challenging due to the stringent upper bound on $\cos(\beta - \alpha)$. A sizable signal significance demands an upper bound on $\tan\beta$, contrary to high scale validity constraints, where no such bound is predicted. An analysis at the 14 TeV LHC including detector effects reveals that H and A of masses around 500 GeV can be simultaneously observed in their respective channels with at least 3σ confidence when the integrated luminosity is 3000 fb^{-1} . The observability improves upon de-escalating the cut-off scale, attaining 5σ statistical significance becomes possible when the cut-off is near 10^{11} GeV .

Radiative return at the muon collider yields sizable production rates of H or A . We have studied the observation their prospects through their subsequent decay to the $b\bar{b}$ final state. Contrary to the results obtained for the LHC, the $\mu^+\mu^-$ machine can lead to a 5σ statistical significance even if the scalar mass is 1 TeV. Thus a certain complementarity of roles between the LHC and a muon collider is noticed. The former has relatively lower mass reach but clearly differentiates the H -peak from the A -peak, while the latter loses this distinction by being forced to look at the $b\bar{b}$ decay mode, though up to higher (pseudo)scalar masses.

7 Acknowledgements

We thank Subhadeep Mondal and Jyotirnanjan Beuria for useful discussions. This work was partially supported by funding available from the Department of Atomic Energy, Government of India, for the Regional Centre for Accelerator-based Particle Physics (RECAPP), Harish-Chandra Research Institute.

References

- [1] **ATLAS** Collaboration, G. Aad *et. al.*, *Observation of a new particle in the search for the Standard Model Higgs boson with the ATLAS detector at the LHC*, *Phys.Lett.* **B716** (2012) 1–29, [[arXiv:1207.7214](https://arxiv.org/abs/1207.7214)].

- [2] **CMS** Collaboration, S. Chatrchyan *et. al.*, *Observation of a new boson at a mass of 125 GeV with the CMS experiment at the LHC*, *Phys. Lett.* **B716** (2012) 30–61, [[arXiv:1207.7235](#)].
- [3] G. Degrandi, S. Di Vita, J. Elias-Miro, J. R. Espinosa, G. F. Giudice, G. Isidori, and A. Strumia, *Higgs mass and vacuum stability in the Standard Model at NNLO*, *JHEP* **08** (2012) 098, [[arXiv:1205.6497](#)].
- [4] D. Buttazzo, G. Degrandi, P. P. Giardino, G. F. Giudice, F. Sala, A. Salvio, and A. Strumia, *Investigating the near-criticality of the Higgs boson*, *JHEP* **12** (2013) 089, [[arXiv:1307.3536](#)].
- [5] M. Gonderinger, H. Lim, and M. J. Ramsey-Musolf, *Complex scalar singlet dark matter: Vacuum stability and phenomenology*, *Phys. Rev. D* **86** (Aug, 2012) 043511.
- [6] M. Gonderinger, Y. Li, H. Patel, and M. J. Ramsey-Musolf, *Vacuum stability, perturbativity, and scalar singlet dark matter*, *Journal of High Energy Physics* **2010** (2010), no. 1 53.
- [7] C.-S. Chen and Y. Tang, *Vacuum stability, neutrinos, and dark matter*, *JHEP* **04** (2012) 019, [[arXiv:1202.5717](#)].
- [8] I. Gogoladze, N. Okada, and Q. Shafi, *Higgs boson mass bounds in a type ii seesaw model with triplet scalars*, *Phys. Rev. D* **78** (Oct, 2008) 085005.
- [9] J. Chakraborty, J. Gluza, T. Jeliski, and T. Srivastava, *Theoretical constraints on masses of heavy particles in left-right symmetric models*, *Physics Letters B* **759** (2016) 361 – 368.
- [10] X.-G. He, H. Phoon, Y. Tang, and G. Valencia, *Unitarity and vacuum stability constraints on the couplings of color octet scalars*, *JHEP* **05** (2013) 026, [[arXiv:1303.4848](#)].
- [11] R. S. Chivukula, A. Farzinia, and E. H. Simmons, *Vacuum stability and triviality analyses of the renormalizable coloron model*, *Phys. Rev. D* **92** (Sep, 2015) 055002.
- [12] J. Baglio, O. Eberhardt, U. Nierste, and M. Wiebusch, *Benchmarks for higgs boson pair production and heavy higgs boson searches in the two-higgs-doublet model of type ii*, *Phys. Rev. D* **90** (Jul, 2014) 015008.
- [13] V. Keus, S. F. King, S. Moretti, and K. Yagyu, *Cp violating two-higgs-doublet model: constraints and lhc predictions*, *Journal of High Energy Physics* **2016** (2016), no. 4 48.
- [14] S. Kanemura, H. Yokoya, and Y.-J. Zheng, *Complementarity in direct searches for additional higgs bosons at the {LHC} and the international linear collider*, *Nuclear Physics B* **886** (2014) 524 – 553.
- [15] L. Basso, A. Lipniacka, F. Mahmoudi, S. Moretti, P. Osland, G. M. Pruna, and M. Purmohammadi, *Probing the charged Higgs boson at the LHC in the CP-violating type-II 2HDM*, *JHEP* **11** (2012) 011, [[arXiv:1205.6569](#)].
- [16] D. Gonçalves and D. López-Val, *Pseudoscalar searches with dileptonic tops and jet substructure*, *Phys. Rev. D* **94** (Nov, 2016) 095005.
- [17] R. Patrick, P. Sharma, and A. G. Williams, *Exploring a heavy charged Higgs using jet substructure in a fully hadronic channel*, *Nucl. Phys.* **B917** (2017) 19–30, [[arXiv:1610.0591](#)].

- [18] J. Li, R. Patrick, P. Sharma, and A. G. Williams, *Boosting the charged Higgs search prospects using jet substructure at the LHC*, *JHEP* **11** (2016) 164, [[arXiv:1609.0264](#)].
- [19] A. Arhrib, R. Benbrik, S. J. D. King, B. Manaut, S. Moretti, and C. S. Un, *Phenomenology of 2HDM with VLQs*, [arXiv:1607.0851](#).
- [20] A. G. Akeroyd *et. al.*, *Prospects for charged Higgs searches at the LHC*, [arXiv:1607.0132](#).
- [21] D. Lopez-Val and J. Sola, *Neutral Higgs-pair production at Linear Colliders within the general 2HDM: Quantum effects and triple Higgs boson self-interactions*, *Phys. Rev.* **D81** (2010) 033003, [[arXiv:0908.2898](#)].
- [22] V. Barger, L. L. Everett, H. E. Logan, and G. Shaughnessy, *Scrutinizing the 125 gev higgs boson in two higgs doublet models at the lhc, ilc, and muon collider*, *Phys. Rev. D* **88** (Dec, 2013) 115003.
- [23] N. Chakrabarty, U. K. Dey, and B. Mukhopadhyaya, *High-scale validity of a two-Higgs doublet scenario: a study including LHC data*, *JHEP* **12** (2014) 166, [[arXiv:1407.2145](#)].
- [24] D. Das and I. Saha, *Search for a stable alignment limit in two-Higgs-doublet models*, *Phys. Rev.* **D91** (2015), no. 9 095024, [[arXiv:1503.0213](#)].
- [25] G. Branco, P. Ferreira, L. Lavoura, M. Rebelo, M. Sher, *et. al.*, *Theory and phenomenology of two-Higgs-doublet models*, *Phys.Rept.* **516** (2012) 1–102, [[arXiv:1106.0034](#)].
- [26] B. Grzadkowski, O. M. Ogreid, and P. Osland, *Diagnosing CP properties of the 2HDM*, *JHEP* **01** (2014) 105, [[arXiv:1309.6229](#)].
- [27] J. Shu and Y. Zhang, *Impact of a CP Violating Higgs Sector: From LHC to Baryogenesis*, *Phys. Rev. Lett.* **111** (2013), no. 9 091801, [[arXiv:1304.0773](#)].
- [28] J. F. Gunion and H. E. Haber, *Conditions for cp violation in the general two-higgs-doublet model*, *Phys. Rev. D* **72** (Nov, 2005) 095002.
- [29] E. A. Paschos, *Diagonal neutral currents*, *Phys. Rev. D* **15** (Apr, 1977) 1966–1972.
- [30] S. L. Glashow and S. Weinberg, *Natural conservation laws for neutral currents*, *Phys. Rev. D* **15** (Apr, 1977) 1958–1965.
- [31] C. S. Kim, Y. W. Yoon, and X.-B. Yuan, *Exploring top quark fenc within 2hdm type iii in association with flavor physics*, *Journal of High Energy Physics* **2015** (2015), no. 12 1–30.
- [32] A. Crivellin, A. Kokulu, and C. Greub, *Flavor-phenomenology of two-Higgs-doublet models with generic Yukawa structure*, *Phys. Rev.* **D87** (2013), no. 9 094031, [[arXiv:1303.5877](#)].
- [33] I. Baum, G. Eilam, and S. Bar-Shalom, *Scalar flavor changing neutral currents and rare top quark decays in a two Higgs doublet model 'for the top quark'*, *Phys. Rev.* **D77** (2008) 113008, [[arXiv:0802.2622](#)].
- [34] G. Cvetič, S. S. Hwang, and C. S. Kim, *Higgs-mediated flavor-changing neutral currents in the general framework with two higgs doublets: An rge analysis*, *Phys. Rev. D* **58** (Oct, 1998) 116003.

- [35] A. G. Akeroyd, A. Arhrib, and E.-M. Naimi, *Note on tree level unitarity in the general two Higgs doublet model*, *Phys.Lett.* **B490** (2000) 119–124, [[hep-ph/0006035](#)].
- [36] J. Horejsi and M. Kladiva, *Tree-unitarity bounds for THDM Higgs masses revisited*, *Eur.Phys.J.* **C46** (2006) 81–91, [[hep-ph/0510154](#)].
- [37] S. Kanemura and K. Yagyu, *Unitarity bound in the most general two Higgs doublet model*, *Phys. Lett.* **B751** (2015) 289–296, [[arXiv:1509.0606](#)].
- [38] I. F. Ginzburg and I. P. Ivanov, *Tree-level unitarity constraints in the most general 2HDM*, *Phys. Rev.* **D72** (2005) 115010, [[hep-ph/0508020](#)].
- [39] S. Kanemura, T. Kubota, and E. Takasugi, *Lee-Quigg-Thacker bounds for Higgs boson masses in a two doublet model*, *Phys.Lett.* **B313** (1993) 155–160, [[hep-ph/9303263](#)].
- [40] P. Ferreira, R. Santos, and A. Barroso, *Stability of the tree-level vacuum in two Higgs doublet models against charge or CP spontaneous violation*, *Phys.Lett.* **B603** (2004) 219–229, [[hep-ph/0406231](#)].
- [41] N. G. Deshpande and E. Ma, *Pattern of symmetry breaking with two higgs doublets*, *Phys. Rev. D* **18** (Oct, 1978) 2574–2576.
- [42] S. Nie and M. Sher, *Vacuum stability bounds in the two-higgs doublet model*, *Physics Letters B* **449** (1999), no. 12 89 – 92.
- [43] **Gfitter Group** Collaboration, M. Baak *et. al.*, *The global electroweak fit at NNLO and prospects for the LHC and ILC*, *Eur.Phys.J.* **C74** (2014) 3046, [[arXiv:1407.3792](#)].
- [44] F. Mahmoudi and O. Stal, *Flavor constraints on the two-Higgs-doublet model with general Yukawa couplings*, *Phys.Rev.* **D81** (2010) 035016, [[arXiv:0907.1791](#)].
- [45] **Particle Data Group** Collaboration, C. Patrignani *et. al.*, *Review of Particle Physics*, *Chin. Phys.* **C40** (2016), no. 10 100001.
- [46] O. Eberhardt, *Fitting the Two-Higgs-Doublet model of type II*, in *Proceedings, 49th Rencontres de Moriond on Electroweak Interactions and Unified Theories*, pp. 523–526, 2014. [[arXiv:1405.3181](#)].
- [47] P. Ferreira, H. E. Haber, and E. Santos, *Preserving the validity of the Two-Higgs Doublet Model up to the Planck scale*, *Phys. Rev.* **D92** (2015) 033003, [[arXiv:1505.0400](#)].
- [48] J. Bernon, J. F. Gunion, H. E. Haber, Y. Jiang, and S. Kraml, *Scrutinizing the alignment limit in two-Higgs-doublet models: $m_h=125\text{GeV}$* , *Phys. Rev.* **D92** (2015), no. 7 075004, [[arXiv:1507.0093](#)].
- [49] H. S. Cheon and S. K. Kang, *Constraining parameter space in type-II two-Higgs doublet model in light of a 126 GeV Higgs boson*, *JHEP* **09** (2013) 085, [[arXiv:1207.1083](#)].
- [50] V. Barger, L. L. Everett, C. B. Jackson, A. D. Peterson, and G. Shaughnessy, *Measuring the two-higgs doublet model scalar potential at lhc14*, *Phys. Rev. D* **90** (Nov, 2014) 095006.
- [51] A. Alloul, N. D. Christensen, C. Degrande, C. Duhr, and B. Fuks, *Feynrules 2.0 a complete toolbox for tree-level phenomenology*, *Computer Physics Communications* **185** (2014), no. 8 2250 – 2300.

- [52] J. Alwall, R. Frederix, S. Frixione, V. Hirschi, F. Maltoni, O. Mattelaer, H. S. Shao, T. Stelzer, P. Torrielli, and M. Zaro, *The automated computation of tree-level and next-to-leading order differential cross sections, and their matching to parton shower simulations*, *JHEP* **07** (2014) 079, [[arXiv:1405.0301](#)].
- [53] T. Sjöstrand, S. Mrenna, and P. Skands, *Pythia 6.4 physics and manual*, *Journal of High Energy Physics* **2006** (2006), no. 05 026.
- [54] J. de Favereau, C. Delaere, P. Demin, A. Giammanco, V. Lemaître, A. Mertens, and M. Selvaggi, *Delphes 3: a modular framework for fast simulation of a generic collider experiment*, *Journal of High Energy Physics* **2014** (2014), no. 2 57.
- [55] **ATLAS** Collaboration, G. Aad *et. al.*, *Search for an additional, heavy Higgs boson in the $H \rightarrow ZZ$ decay channel at $\sqrt{s} = 8$ TeV in pp collision data with the ATLAS detector*, *Eur. Phys. J.* **C76** (2016), no. 1 45, [[arXiv:1507.0593](#)].
- [56] **CMS** Collaboration, V. Khachatryan *et. al.*, *Search for a pseudoscalar boson decaying into a Z boson and the 125 GeV Higgs boson in $^+b\bar{b}$ final states*, *Phys. Lett.* **B748** (2015) 221–243, [[arXiv:1504.0471](#)].
- [57] R. N. Hodgkinson, D. Lopez-Val, and J. Sola, *Higgs boson pair production through gauge boson fusion at linear colliders within the general 2HDM*, *Phys. Lett.* **B673** (2009) 47–56, [[arXiv:0901.2257](#)].
- [58] H. Abramowicz *et. al.*, *The International Linear Collider Technical Design Report - Volume 4: Detectors*, [arXiv:1306.6329](#).
- [59] N. Chakrabarty, T. Han, Z. Liu, and B. Mukhopadhyaya, *Radiative return for heavy higgs boson at a muon collider*, *Phys. Rev. D* **91** (Jan, 2015) 015008.